buildings

MDPI

Article

A Constitutive Model for Circular and Square Cross-Section Concrete Confined with Aramid FRP Laminates

Yeou-Fong Li [1,*], Bo-Yu Chen [1], Jin-Yuan Syu [1], Gobinathan Kadagathur Ramanathan [1], Wei-Hao Lee [2], Chih-Hong Huang [3] and Man-Hoi Lok [4]

[1] Department of Civil Engineering, National Taipei University of Technology, 1, Sec. 3, Chung-Hsiao E. Rd., Taipei 10608, Taiwan; harris860612@gmail.com (B.-Y.C.); t9679010@ntut.org.tw (J.-Y.S.); gobiram0017@gmail.com (G.K.R.)
[2] Institute of Mineral Resources Engineering, National Taipei University of Technology, 1, Sec. 3, Chung-Hsiao E. Rd., Taipei 10608, Taiwan; whlee@ntut.edu.tw
[3] Department of Architecture, National Taipei University of Technology, 1, Sec. 3, Chung-Hsiao E. Rd., Taipei 10608, Taiwan; huangch@ntut.edu.tw
[4] Department of Civil and Environmental Engineering, Faculty of Science and Technology, University of Macau, Avenida da Universidade Taipa, Macau 999078, China; mhlok@um.edu.mo
* Correspondence: yfli@mail.ntut.edu.tw

Abstract: Fiber-reinforced polymer (FRP) has been used for seismic retrofitting and structural reinforcement over recent decades. Numerous researchers have created stress–strain models based on experimental data to predict the mechanical properties of FRP-confined concrete. In this study, circular and square cross-section specimens with different design concrete strength were prepared, and the compressive strength of the specimens confined with different layers of aramid FRP (AFRP) were measured in compressive tests. A constitutive model was proposed to simulate the uniaxial compressive stress–strain relationship of the AFRP-confined concrete, which was derived from the Mohr–Coulomb failure envelope theory, and the corresponding axial strain was determined from the regression analysis. The internal friction angle of the proposed constitutive model was determined for the cylindrical concrete specimens confined with one and two layers of AFRP. The compressive strength of one and two layers of AFRP-confined concrete specimens were used to obtain the parameters of the constitutive model; the absolute average error between experimental and predicted compressive strength was 7.01%. Then, the constitutive model was used to predict the strength of a three-layer AFRP-confined concrete specimen, and the absolute average error was 4.95%. The cross-sectional shape coefficient of the square concrete specimen was obtained analytically. Substituting the cross-sectional shape coefficient into the proposed constitutive model, the average absolute error of the square cross-section concrete specimen was about 3.84%. The results indicated that the proposed constitutive model can predict the compressive strength of circular and square cross-section concrete specimens confined with AFRP.

Keywords: aramid; fiber-reinforced polymer (FRP); Mohr–Coulomb failure envelope; constitutive model; cross-sectional shape coefficient

Citation: Li, Y.-F.; Chen, B.-Y.; Syu, J.-Y.; Ramanathan, G.K.; Lee, W.-H.; Huang, C.-H.; Lok, M.-H. A Constitutive Model for Circular and Square Cross-Section Concrete Confined with Aramid FRP Laminates. *Buildings* **2023**, *13*, 2895. https://doi.org/10.3390/buildings13112895

Academic Editor: Andreas Lampropoulos

Received: 23 October 2023
Revised: 10 November 2023
Accepted: 17 November 2023
Published: 20 November 2023

1. Introduction

The deterioration of concrete structures is usually the result of inadequate maintenance, especially in highly seismic regions. Natural disasters such as earthquakes, hurricanes, and tsunamis could destroy reinforced concrete (RC) structures; therefore, increasing the strength of RC structures in the most efficient way has become an important issue. The existing retrofitting methods include steel plate jackets and fiber-reinforced polymer (FRP) jackets.

The advantages of FRP include a high elastic modulus; corrosion, acid, and alkali resistance; high strength; and light weight. The compressive strength of concrete specimens

could be enhanced when confined with FRP material, and the axial strain would increase as well [1–5]. In the current practice, carbon-fiber-reinforced polymer (CFRP) was one of the most popular FRP materials for repairing and retrofitting RC structural members [6–8].

The experimental results from recent studies showed that the ultimate axial compressive strength and the corresponding strain were effectively improved when the low-strength concrete specimens were confined with carbon fiber composite materials [9–11]. Zhang et al. (2023) explored the compressive strength properties of CFRP and GFRP confined geopolymer concrete. The results indicated that, due to the higher tensile strength and elastic modulus of CFRP, the restraining effects of CFRP were greater than those of GFRP [12].

Recently, aramid fiber has attracted more attention from many researchers in civil engineering because it has the characteristics of better corrosion resistance and higher specific strength, and its elongation is higher than that of carbon fiber. Some researchers used aramid FRP (AFRP) to wrap RC cylindrical members; the results showed that the load-bearing capacity of RC cylindrical members was improved by increasing the AFRP layers [13–19]. Although the maximum tensile strength of aramid fiber was not as high as that of carbon fiber, the elongation was twice the latter, which could significantly improve the deformation and energy absorption of the concrete under loadings. The material properties of the commonly used fibers for FRP repair and retrofit are shown in Table 1 [20–25].

Table 1. Material properties of fibers.

Properties	Fiber			
	Aramid	**Carbon**	**Glass**	**Basalt**
Density (g/cm^3)	1.44	1.78	2.48~2.76	2.65
Tensile Strength (MPa)	2500~3100	3500~6000	1400~2500	3800~4840
Elastic Modulus (GPa)	60~120	230~600	70~80	93.1~110
Elongation (%)	2.1~4.5	1.5~2.0	2.5~3.5	3.1

For CFRP-confined concrete, the lateral confinement stress of CFRP was usually 15 to 30 times the lateral confinement stress of steel reinforcement (spiral); therefore, the axial compressive strength of the CFRP-confined concrete was also higher than that of steel reinforcement confined concrete. To estimate the peak uniaxial compressive strength of FRP-confined concrete accurately, a more effective and accurate formula must be established. In the last few decades, the constitutive models of confined concrete have been researched extensively. Mander et al. proposed a functional equation to present the stress–strain relationship and introduced the "effectiveness coefficient" of reinforced concrete specimens with circular, square, and rectangular cross-sections [26,27]. Mirmiran and Shahawy (1997) proposed an equation to predict the peak strength of glass FRP (GFRP) confined concrete [28]. Razvi and Saatcioglu (1998) proposed a constraint equation for high-strength concrete [29]. Li's research proposed the constitutive models for normal-strength and low-strength cylindrical concrete confined with CFRP, which was adopted from the Mohr–Coulomb failure theory to predict the compressive strength of CFRP-confined concrete [30–34]. Wang et al. (2012) found that the CFRP-confined-square-cross-section column failed suddenly via CFRP rupture at the corner of the column, and a modified confinement pressure model was proposed which considered the influence of cross-section size, effective rupture strain of CFRP, as well as hoop reinforcement [35]. Some studies presented the results of experimental studies on concrete cylinders confined with CFRP composites and proposed confinement models for cylindrical concrete members wrapped with FRP [36–39]. Toufigh et al. (2019) investigated the mechanical properties of a polymer concrete beam/pile confined with CFRP. The result showed that the ductility and bending capacity were enhanced when CFRP sleeves were filled with polymer concrete [40].

Djafar-Henni and Kassoul (2018) measured the compressive stress–strain relationships of 81 concrete cylinders confined with AFRP wraps and compared them with the proposed

model, which agrees with experimental curves of AFRP-confined concrete cylinders [41]. Arabshahi et al. (2020) proposed a model using an evolutionary algorithm named multi-expression programming; the stress–strain model predicted the behavior of AFRP-confined concretes with good accuracy [42]. In addition, due to the effect of the corner radius of FRP confined square concrete specimens, the constitutive model was different from the circular specimens when forecasting the actual situation. Li et al. (2019) tried to rebuild a well-established stress–strain model for the FRP confined square concrete specimens based on the circular ones [11]. However, the stress–strain model of FRP confined square cross-section concrete specimens was not precise enough to match the experimental results [11,43]. Diboune et al. (2022) proposed a model to predict the ultimate strength, ultimate strain, and axial stress–strain relationship of square and rectangular concrete columns confined with CFRP wraps. The proposed model provides good accuracy compared with the other existing models [44].

The majority of the prediction models from the references were developed using experimental regression. Consequently, this study aims to build a constitutive model for AFRP-confined concrete specimens with circular and square cross-sections based on the Mohr–Coulomb failure envelope theory. The experimental compressive stress–strain relationships of AFRP-confined concrete were used to obtain the parameters of the proposed constitutive model and then compared with other studies to illustrate the accuracy of the proposed constitutive model.

2. Materials and Fabrication of Test Specimens

This section introduces the materials used in the preparation of AFRP-confined concrete specimens, including the material characteristics of aramid sheets and epoxy resin. The proportions of cement, sand, and aggregates are also listed in this section.

2.1. Aramid Fiber

Aramid fiber is a high modulus, low density, high specific strength, and organic synthetic high-tech fiber with good abrasion resistance. The applications of aramid fiber include military equipment, automotive components, flame-resistant clothing, sports equipment, etc. Although the strength of aramid fiber was slightly lower than that of carbon fiber, its elongation was higher. The unidirectional aramid fiber fabric (Kevlar® 29, DuPont, Richmond, VA, USA) was used in this study. The mechanical properties of aramid fiber were tested to the standards shown in Table 2.

Table 2. Material properties of aramid fiber (Kevlar® 29) unidirectional sheet.

Properties	Value	Test Standard
Fiber areal weight, FAW (g/m^2)	225.0	ASTM D3776
Young's modulus (GPa)	128.5	ASTM D3039
Tensile strength (MPa)	2188.5	ASTM D3039
Elongation (%)	3.6	ASTM D3039

2.2. Epoxy Resin

Epoxy resin has the characteristics of excellent moisture resistance and low shrinkage during curing, and it may improve the mechanical strength of the composite. In this study, the weight mixing ratio of epoxy resin and hardener was 2:1 to produce SB838 epoxy resin (Sam Bond Int'l Corp., Taiwan).

2.3. Concrete Specimen Preparations

Aggregate is the main component resisting compressive stress in concrete. In this study, the weight ratio of coarse aggregates (3/8″ and 6/8″ gravel) was 1:1. The fineness modulus (F.M.) of fine aggregates and coarse aggregates were 3.05 and 7.5, respectively; the fineness modulus of all aggregates was 5.42. The concrete specimens were prepared with different water to cement (w/c) ratios, and the mixing ratio of cement, sand, and aggregate

in the concrete was 1:1.81:4.52. A total of 156 concrete specimens were tested in this study. The concrete specimens had different cross-sections: 120 cylindrical concrete specimens (Ø10 × 20 cm and Ø15 × 30 cm) with five different w/c ratios (0.50, 0.55, 0.60, 0.65, and 0.70) and 36 square cross-section concrete specimens (20 cm in height and 10 cm in width) with three different w/c ratios (0.50, 0.55, and 0.65). Each of the unconfined and confined (one to three layers) concrete specimens with different w/c ratios included three specimens.

The concrete specimens were wrapped with AFRP laminates by hand and layered-up on the 18th day of curing. The epoxy was applied to the surface of concrete specimens and cured at ambient temperature for several hours. The epoxy resin was applied to the surface of the specimen to adhere to and saturate the aramid fiber sheet. The aramid fiber was saturated in the epoxy resin by using a paintbrush, and the remaining epoxy was squeezed out by using a flat plastic scraper. The overlay length is more than 10 cm for each layer of the AFRP laminate confinement, as shown in Figure 1. Before applying the next layer of the AFRP laminate, it would take 24 h for the epoxy resin to cure, and then the above steps were repeated for the required number of layers. Finally, the AFRP-confined concrete with epoxy was cured for more than 7 days at ambient temperature.

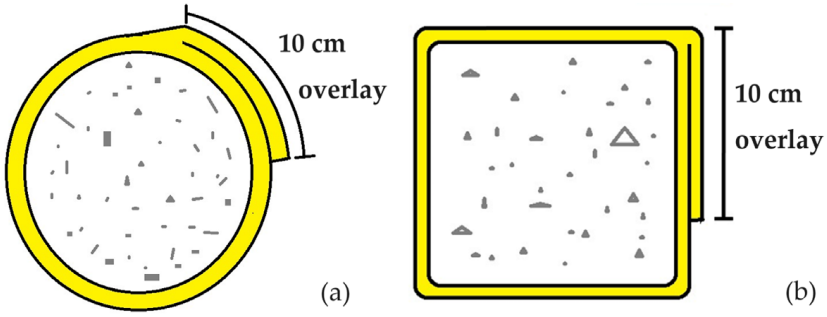

Figure 1. Concrete specimen wrapping with AFRP confinement: (**a**) cylindric specimen and (**b**) square specimen.

2.4. Compressive Test

The compressive strength of the circular (Ø10 × 20 cm and Ø15 × 30 cm) and square cross-section concrete specimens with and without AFRP confinement are presented and discussed in this section. The AFRP-laminate-confined concrete specimens were tested with the universal testing machine at the Department of Civil Engineering, National Taipei University of Technology. As per the ASTM C39/C39M-01 standard [45], the loading rate of the actuator was 0.21 MPa/s. In addition, the loading process was stopped when the axial load was decreased to 70 percent of compressive strength. In the compressive test, a load cell (WF 17120, Wykeham Farrance, Milan, Italy) with a 500 kN capacity and strain gauges (KFGS-20-120-C1 L3M2R, KYOWA, Tokyo, Japan) were utilized. Additionally, a data acquisition system (KL-10, Geomaster Group, Tianjin, China) was used to obtain the force and strain information during compressive testing.

3. Results

3.1. Unconfined Concrete Specimens (Benchmark)

In this subsection, the compressive test results of unconfined concrete specimens with five different designed strengths and three different cross-sections are listed in Table 3. Five different designed compressive strengths for the specimens were controlled with different w/c ratios with the compressive strength ranging from 20 MPa to 34 MPa.

Table 3. Average axial compressive strength of the unconfined concrete specimens.

Specimen *	Average Compressive Strength (MPa)	Specimen *	Average Compressive Strength (MPa)	Specimen *	Average Compressive Strength (MPa)
C10W50	34.4	C15W50	33.1	S10W50	33.1
C10W55	31.3	C15W55	30.2	S10W55	29.6
C10W60	27.8	C15W60	27.1	S10W65	24.4
C10W65	24.1	C15W65	23.4		
C10W70	21.0	C15W70	21.3		

* C is the circular specimen, and the number afterwards is the cross-section diameter of the specimen; S is the square specimen, and the number afterwards is the cross-section width of the specimen; W is the water/cement ratio (w/c) of the specimen in %. For example, C10W50 is the specimen with the diameter of 10 cm and a water/cement ratio of 50%.

3.2. Confined Concrete Specimens Ø10 × 20

The compressive stress–strain relationships and ultimate lateral strains were measured for the Ø10 × 20 cm confined concrete specimens. Table 4 shows the compression test results for cylindrical concrete specimens with different w/c ratios and confined with different layers of AFRP. The AFRP-confined layers were increased from one to three layers, and then the compressive strength for five different w/c ratios (0.5, 0.55, 0.6, 0.65, and 0.7) were increased by 28~134%, 61~181%, 60~206%, 89~271%, 101~259%, respectively. The ultimate lateral strains are also shown in Table 4. The lateral strain was measured by using strain gauges; two strain gauges were mounted on the surface, one-third and two-thirds of the height for each cylindrical concrete specimen measured from the bottom.

Table 4. Experimental results of the AFRP-confined cylindrical specimens (Ø10 × 20).

Specimen *	Compressive Strength (MPa)		Ultimate Compressive Axial Strain		Measured Ultimate Lateral Strain
	Test	Avg. Value/ Increment (%)	Test	Avg. Value	
C10W50L1	40.7; 47.7; 43.7	44.0/28	0.0132; 0.0106; 0.0126	0.0121	0.0135; 0.0147; 0.0181
C10W50L2	64.5; 64.0; 69.1	65.9/91	0.0191; 0.0185; 0.0170	0.0182	0.0115; 0.0133; 0.0159
C10W50L3	77.5; 80.9; 83.8	80.7/134	0.0228; 0.0235; 0.0191	0.0218	0.0172; 0.0184; 0.0176
C10W55L1	50.5; 51.7; 49.4	50.5/61	0.0114; 0.0121; 0.0128	0.0121	0.0158; 0.0135; 0.0148
C10W55L2	72.2; 67.1; 73.9	71.1/126	0.0145; 0.0122; 0.0173	0.0147	0.0209; 0.0186; 0.0180
C10W55L3	88.5; 90.4; 86.2	88.4/181	0.0171; 0.0187; 0.0189	0.0183	0.0136; 0.0142; 0.0113
C10W60L1	43.3; 47.7	45.5/60	0.0129; 0.0126	0.0128	-
C10W60L2	72.1; 74.8; 78.4	75.1/170	0.0188; 0.0201; 0.0208	0.0199	-
C10W60L3	83.2; 90.6; 81.7	85.2/206	0.0205; 0.0218; 0.0191	0.0205	-
C10W65L1	44.9; 46.9; 45.2	45.7/89	0.0112; 0.0131; 0.0128	0.0124	0.0113; 0.0175; 0.0198
C10W65L2	65.3; 70.5; 71.6	69.1/187	0.0161; 0.0186; 0.0153	0.0167	0.0155; 0.0163; 0.0143
C10W65L3	93.9; 84.9	89.4/271	0.0244; 0.0196	0.0220	0.0175; 0.0166
C10W70L1	40.6; 44.6; 41.6	42.3/101	0.0142; 0.0161; 0.0171	0.0158	-
C10W70L2	63.1; 59.7; 55.7	59.5/183	0.0199; 0.0211; 0.0249	0.0220	-
C10W70L3	74.3; 79.6; 72.1	75.33/259	0.0250; 0.0282; 0.0290	0.0274	-

* C is the circular specimen, and the number afterwards is the cross-section diameter of the specimen in cm; W is the water/cement ratio (w/c) of the specimen in %.; L—number of AFRP confined layers (1~3). For example, C10W50L1 represents a specimen with a water/cement ratio of 50%, a diameter of 10 cm, and confinement using one layer of AFRP.

As the water–cement ratio increases, the compressive strength decreases; whereas, as the number of confinement layers increases, the compressive strength increases. The axial stress–strain relationships of the unconfined C10W50 and confined C10W50 with one to three layers of AFRP are shown in Figure 2a–d, respectively. The AFRP confinement improves the axial strain capacity of concrete significantly.

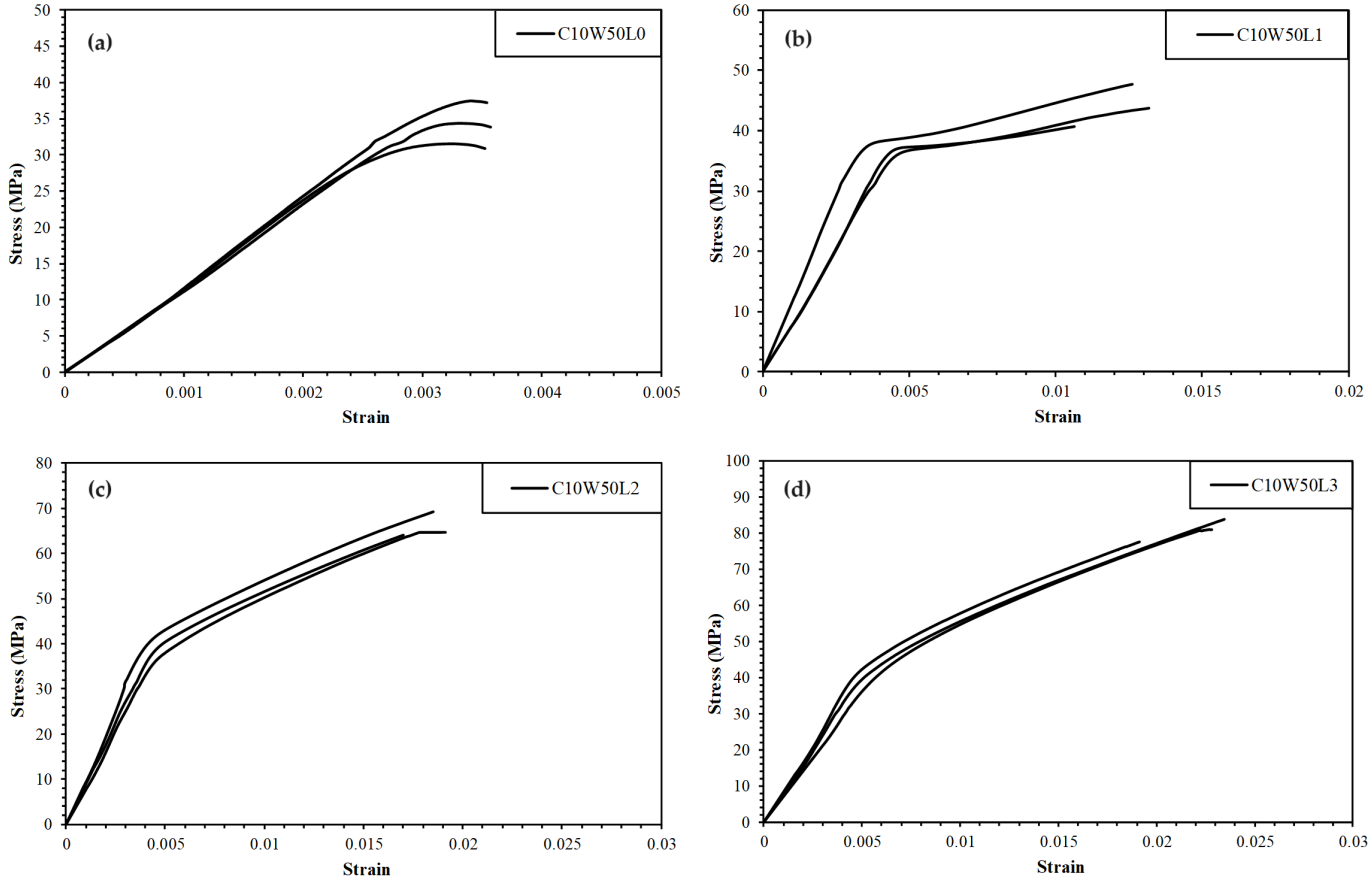

Figure 2. Compressive stress–strain relationships. (**a**) C10W50L0, (**b**) C10W50L1, (**c**) C10W50L2, and (**d**) C10W50L3.

3.3. Confined Concrete Specimens Ø15 × 30

In this subsection, the compression test results and the failure mode of AFRP-confined concrete specimens are discussed. Table 5 shows the compression test result of cylindrical concrete specimens confined with one to three layers of AFRP. As shown in Table 5, the compressive strength increased with the increasing number of AFRP layers, and the increasing percentage for the five different w/c ratios (0.5, 0.55, 0.6, 0.65, and 0.7) were 26~99%, 32~116%, 36~128%, 42~157%, and 68~190%, respectively. The enhancement effect for Ø15 × 30 specimens was similar to that in Ø10 × 20 specimens, in which the AFRP confinement improved the compressive strength of the specimens with high w/c content better than for specimens with lower w/c content. However, the strength increasing percentage was lower compared with Ø10 × 20 specimens because the effective lateral confined stress (f_l) of AFRP decreased with the increased diameter of the cylindrical concrete specimens. The influence of both the effect of confinement (ranging from one to three layers of AFRP) and the diameter (Ø10 and Ø15) on the compressive performance of the concrete specimens is elucidated in Equations (3) and (4) in Section 4.1. Consequently, it is evident that concrete members with larger diameters require the incorporation of more layers of FRP confinement to achieve the same level of strength enhancement.

Table 5. Compression test results of AFRP-confined cylindrical concrete specimens (Ø15 × 30).

Specimen *	Compressive Strength (MPa)	Avg. Compressive Strength (MPa)	Strength Increment (%)	Measured Ultimate Lateral Strain
C15W50L1	42.6; 41.3; 41.3	41.7	26	0.0200; 0.0258; 0.0247
C15W50L2	56.1; 49.4; 54.2	53.2	61	0.0251; 0.0208; 0.0239
C15W50L3	65.1; 67.5; 65.4	66.0	99	0.0155; 0.0201; 0.0159
C15W55L1	40.4; 39.1; 40.0	39.8	32	0.0193; 0.0200; 0.0189
C15W55L2	53.2; 51.6; 51.0	51.9	72	0.0201; 0.0189; 0.0199
C15W55L3	63.2; 65.4; 66.9	65.2	116	0.0193; 0.0180; 0.0186
C15W60L1	37.5; 36.3; 36.8	36.9	36	0.0113; 0.0189; 0.0136
C15W60L2	53.0; 49.0; 50.5	50.8	87	0.0143; 0.0156; 0.0157
C15W60L3	63.2; 62.4; 60.3	62.0	128	0.0183; 0.0203; 0.0192
C15W65L1	34.0; 33.0; 32.5	33.2	42	0.0140; 0.0230; 0.0185
C15W65L2	47.9; 49.4; 49.4	48.9	109	0.0179; 0.0194; 0.0185
C15W65L3	62.5; 58.0; 59.6	60.0	157	0.0169; 0.0233; 0.0188
C15W70L1	32.9; 35.9; 36.1	35.0	68	0.0199; 0.0201; 0.0257
C15W70L2	47.6; 47.7; 45.0	46.8	119	0.0205; 0.0247; 0.0239
C15W70L3	60.9; 62.6; 61.8	61.8	190	0.0200; 0.0157; 0.0198

* C—circular concrete specimens; 15—diameter of circular specimen (cm); W—w/c ratio (%); L—number of AFRP layers (1~3).

The post-test photographs of confined and unconfined cylindrical concrete specimens after the uniaxial compressive test are shown in Figure 3. Figure 3a shows the shear failure of an unconfined cylindrical concrete specimen. Shearing failure with spalling appeared in the AFRP-confined concrete specimens as shown in Figure 3b–d. The shear with spalling failure was more pronounced when increasing the number of the AFRP layers. As seen from the test results, the deformation of the concrete specimen was not uniform, and the measured lateral strains exhibit variation.

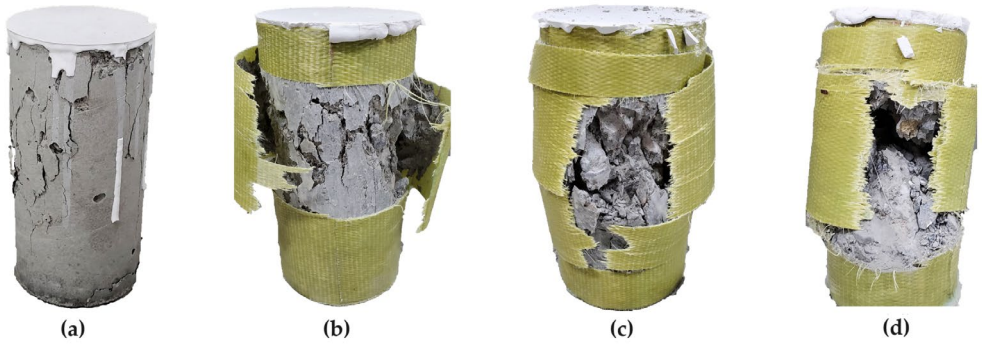

Figure 3. Post-test photographs of C15W60 specimens confined with one, two, and three layers of AFRP after the uniaxial compressive test: (**a**) C15W60, (**b**) C15W60L1, (**c**) C15W60L2, and (**d**) C15W60L3.

3.4. Confined Square Cross-Section Concrete Specimens

The axial stress–strain relationships of the square cross-section concrete specimens (S10W65) without and with AFRP confinement are shown in Figure 4a–d. The confined concrete attained brittle failure before the AFRP rupture, and the measured AFRP-confined strain was less than the strain obtained from the coupon axial test. The compressive strength of the square concrete specimen was enhanced with one to three layers of AFRP confinement from about 24% to 139%, as shown in Table 6. The experimental compressive results and lateral strain of AFRP-confined square concrete specimens are also listed in Table 6.

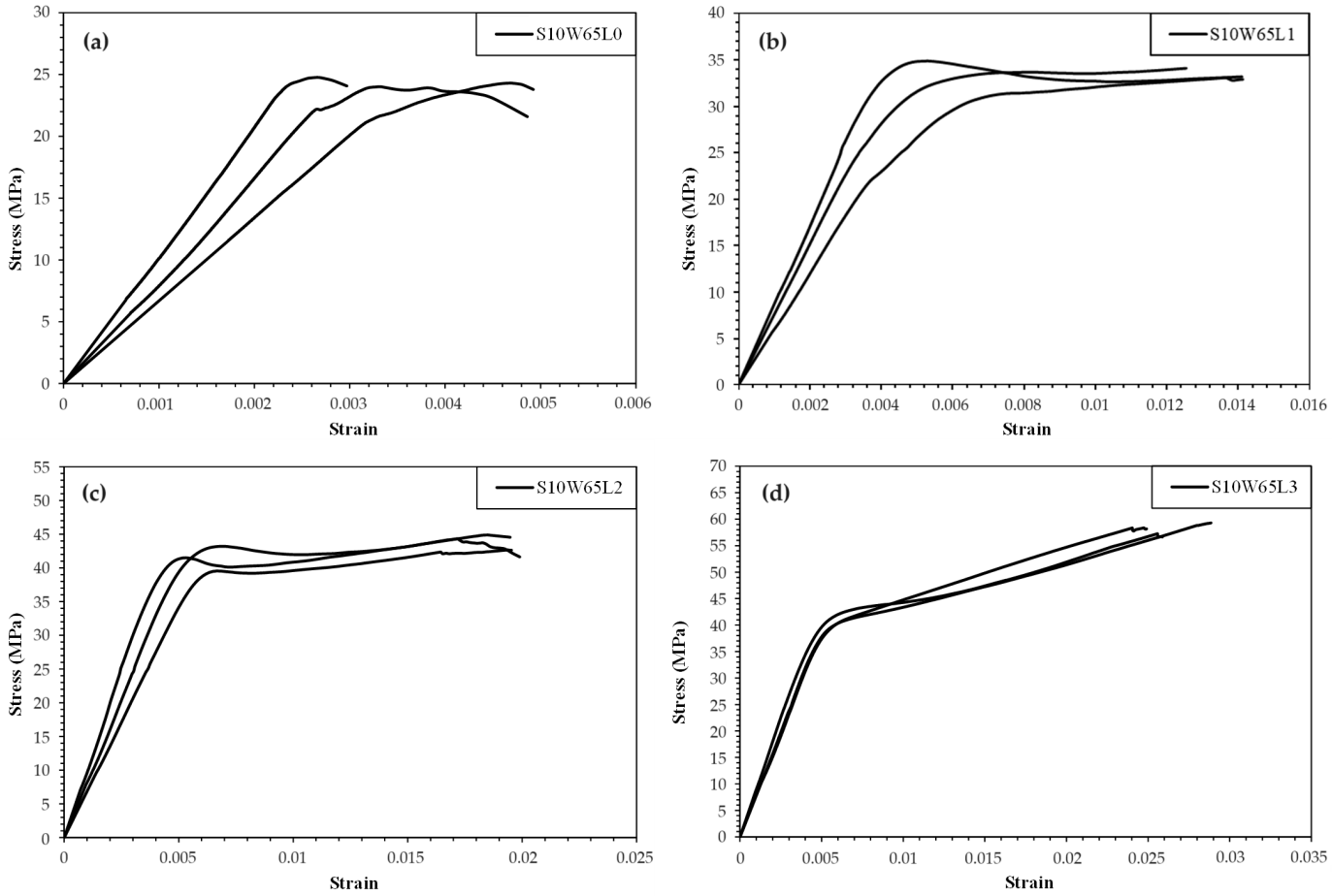

Figure 4. Compressive stress–strain relationships (**a**) S10W65L0, (**b**) S10W65L1, (**c**) S10W65L2, and (**d**) S10W65L3.

Table 6. Experimental results for the AFRP-confined square specimens.

Specimen *	Compressive Strength (MPa)		Ultimate Compressive Axial Strain		Measured Ultimate Lateral Strain
	Test	Avg. Value/ Increment (%)	Test	Avg. Value	
S10W50L1	41.8; 41.6; 39.7	41.0/24	0.0106; 0.0104; 0.0114	0.0108	0.0138; 0.0200; 0.0189
S10W50L2	50.8; 51.2; 52.5	51.5/56	0.0174; 0.0151; 0.0172	0.0166	0.0188; 0.0165; 0.0123
S10W50L3	62.9; 61.5; 62.2	62.2/88	0.0225; 0.0217; 0.0226	0.0223	0.0176; 0.0178; 0.0183
S10W55L1	41.9; 38.8; 37.6	39.4/33	0.0119; 0.0114; 0.0105	0.0112	0.0185; 0.0144; 0.0158
S10W55L2	46.8; 48.9; 44.2	46.6/57	0.0171; 0.0197; 0.0153	0.0174	0.0128; 0.0168; 0.0166
S10W55L3	61.9; 58.3; 62.2	60.8/105	0.0180; 0.0238; 0.0225	0.0214	0.0137; 0.0173; 0.0133
S10W65L1	34.9; 33.1; 34.1	34.0/40	0.0128; 0.0127; 0.0113	0.0123	0.0218; 0.0140; 0.0181
S10W65L2	44.2; 42.6; 44.9	43.9/80	0.0180; 0.0177; 0.0174	0.0177	0.0141; 0.0108; 0.0153
S10W65L3	59.3; 58.3; 57.2	58.3/139	0.0261; 0.0216; 0.0230	0.0236	0.0081; 0.0149; 0.0146

* S—square cross-section concrete specimens; 10—edge length of the square (cm); W—w/c ratio (%); L—number of AFRP layers (1~3).

As seen in Table 6, the compressive strength of AFRP-confined concrete specimens was enhanced by increasing the layers of AFRP. From the experimental results, it was observed that the enhancement effects for AFRP-confined square cross-section concrete specimens were not as good as for the cylindrical specimens. The square cross-section concrete specimens tend to produce more confining stress concentrated around the corners and less confining stress at the edges. Therefore, the confining stress was not uniform for the square cross-section specimens.

The failure photos of the unconfined and confined square cross-section concrete specimens are shown in Figure 5. It can be seen that the AFRP ruptured around the corners of the square cross-section concrete specimens, and this was most likely caused by the confining stresses of the square cross-section concrete specimens concentrating around the corners.

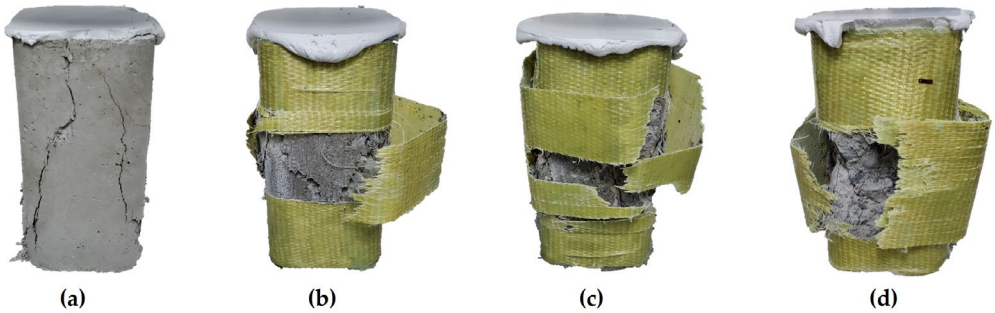

Figure 5. Post-test photographs of S10W65 specimens confined with 1, 2, and 3 layers of AFRP: (**a**) S10W65, (**b**) S10W65L1, (**c**) S10W65L2, and (**d**) S10W65L3.

3.5. Strain Energy

The strain energy (E_s) was defined as the area of the stress–strain relationship curve multiplied by the volume of the specimen as follows.

$$E_s = \sum_{i=1}^{m-1} \left(\frac{\sigma_i + \sigma_{i+1}}{2} \right) \times (\varepsilon_{i+1} - \varepsilon_i) \times V \quad (1)$$

where m is the number of compressive stress data recorded via the universal test machine; σ_i and ε_i are the compressive stress and strain of the concrete specimens at point i; V is the volume of the specimens.

Figures 6 and 7 summarize the strain energy of the cylindrical concrete specimens (Ø10 × 20) and the square concrete specimens. Compared with the unconfined specimens, the strain energy increase percentages for one to three layers of AFRP-confined cylindrical specimens and square specimens were between 466% to 2185% and 314% to 1621%, respectively. It could be concluded that the AFRP confinement significantly enhanced the strain energy capacity of concrete specimens.

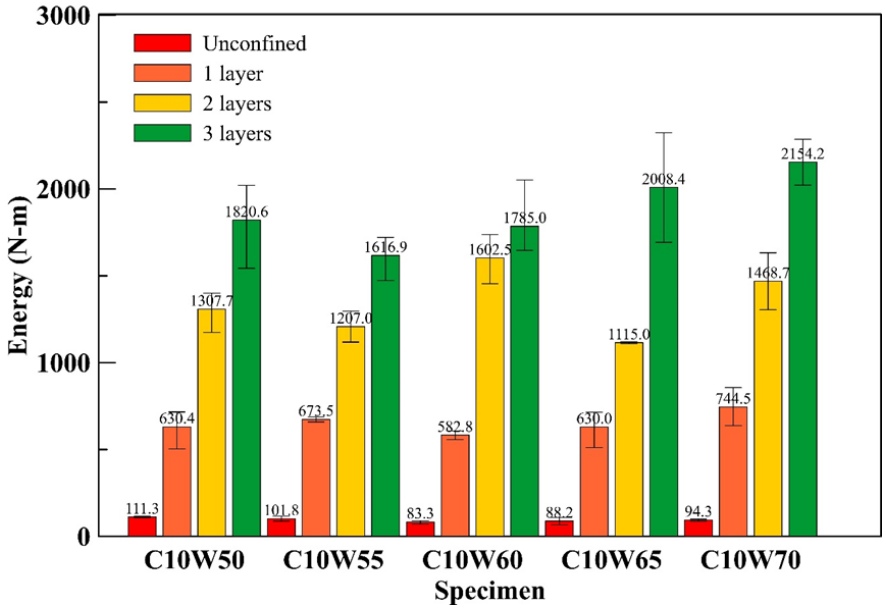

Figure 6. The strain energy of the cylindrical concrete specimens (Ø10 × 20).

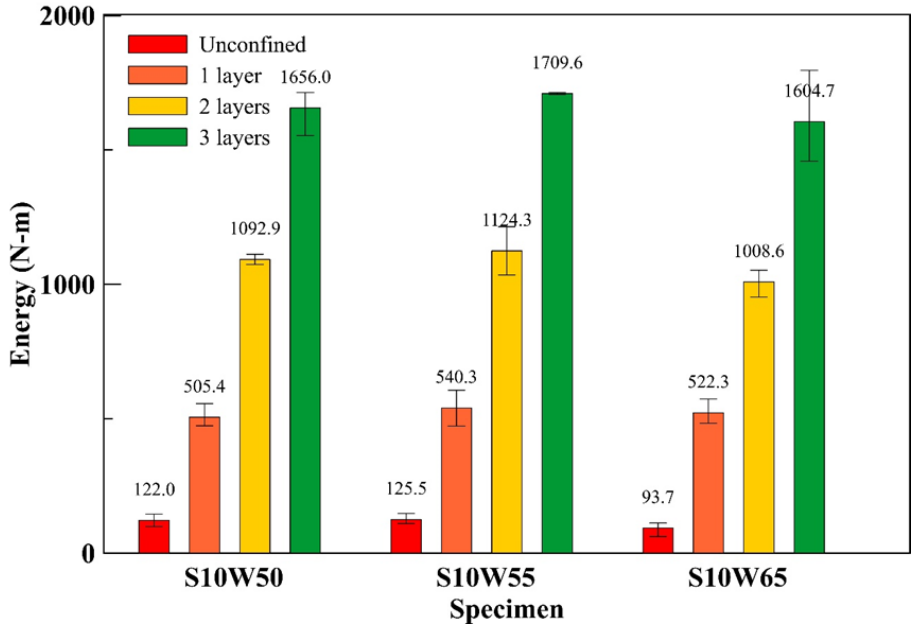

Figure 7. The strain energy of square cross-section concrete specimens.

4. Constitutive Model for AFRP-Confined Concrete

The proposed constitutive model for confined concrete consists of the stress–strain relationship from the initial point to the compressive strength and corresponding strain; the compressive strength value was adopted from the Mohr–Coulomb failure criterion, and the corresponding strain was determined with regression analysis from the experimental data.

4.1. Constitutive Model for Compressive Strength of the Confined Concrete

The compressive strength of confined concrete was adopted from the Mohr–Coulomb failure criterion, and it is incorporated in the following equation:

$$\sigma_1 = C_0 + \sigma_3 tan^2\left(45^0 + \frac{\phi}{2}\right) \quad (2)$$

where σ_1 is the uniaxial compressive strength of rock; σ_3 is the lateral confining stress; ϕ is the internal friction angle; and C_0 is the uniaxial compressive strength without lateral confinement. It was used as a constitutive model to predict the peak compressive strength of concrete confined with AFRP materials.

The mechanical behavior of concrete specimens confined with the AFRP is similar to rocks confined with lateral water pressure. Therefore, the proposed constitutive model can be expressed as follows:

$$f'_{cc} = f'_c + f_l tan^2\left(45^0 + \frac{\phi}{2}\right) \quad (3)$$

where f'_{cc} is the compressive strength of the confined concrete; f'_c is the compressive strength of the unconfined concrete; ϕ is the internal friction angle of concrete; and f_l is the effective lateral confining stress of AFRP, which could be described with the following equation:

$$f_l = \frac{2 \times n \times t \times E_{kf} \times \varepsilon_{kf} \times k_c}{D} \quad (4)$$

where n is the number of AFRP wrapping layers; t is the thickness of a single AFRP layer; E_{kf} is the elastic modulus of AFRP; ε_{kf} is the ultimate lateral strain of AFRP measured from the compressive test; k_c is a cross-section shape factor; and D is the diameter of

the specimen. In this study, the internal friction angle was a function of the compressive strength and was expressed as follows:

$$\phi = A^0 + B^0(f_c') \leq 45^0 \quad (5)$$

Tables 4 and 5 show the measured lateral strains (ε_{kf}) of cylindrical specimens wrapped with different layers of AFRP laminates, and the maximum lateral strain was about 2.5%. The elastic modulus (E_{cf}) and thickness of one-layer AFRP (t) were obtained from Table 2. The lateral confining stress (f_l) of AFRP could be determined by substituting the parameters ε_{kf}, n, E_{cf}, and t as shown in Equation (4). For one to three layers of AFRP-confined cylindrical specimens, the calculated effective lateral confined stresses for specimens with a diameter of 10 cm were 8.84, 17.69, and 26.53 MPa, and for specimens with a diameter of 15 cm were 5.90, 11.79, and 17.69 MPa, respectively.

In this study, the specimens confined with one and two layers of AFRP were used as control variables of the analysis and then used to predict the compressive strength of specimens confined with three layers of AFRP. From Equation (5), the A^0 and B^0 were determined from experimental data from the regression analysis, as shown in Tables 4 and 5; the values of A^0 and B^0 were 20 and 0.002, respectively.

The coefficient of determination (R^2) was used to assess the performance of the proposed constitutive models for AFRP-confined concrete specimens and is expressed as Equation (6).

$$R^2 = \left(\frac{\sum(x-\overline{x})(y-\overline{y})}{\sqrt{\sum(x-\overline{x})^2 \sum(y-y)^2}} \right)^2 \quad (6)$$

where x and y are experimental compressive strength and proposed compressive strength from Equation (3); and $\overline{x}$ and $\overline{y}$ are the average of experimental compressive strength and proposed compressive strength, respectively.

Substituting the compressive strength of the unconfined concretes (f'_c), the effective lateral confining stress of AFRP (f_l), and the internal friction angle (ϕ) into Equation (3), the compressive strength (f'_{cc}) of the proposed constitutive model can be obtained. The average absolute error was 7.01% as shown in Table 7, and the R^2 for the proposed constitutive model and the experimental compressive results was 0.86.

Table 7. Experimental and proposed constitutive model for compressive strength of the specimens confined with one and two layers of AFRP confinement.

Specimen *	Experimental Compressive Strength (MPa)		Proposed Constitutive Model Compressive Strength (Mpa)	Error (%)
	Test	Avg. Value		
C10W50L1	40.7; 47.7; 43.7	44.0	52.5	28.99; 10.06; 20.14
C10W50L2	64.5; 64.0; 69.1	65.9	70.6	9.46; 10.31; 2.17
C10W55L1	50.5; 51.7; 49.4	50.5	49.4	−2.18; −4.45; 0.0
C10W55L2	72.2; 67.1; 73.9	71.1	67.5	−6.51; 0.60; −8.66
C10W60L1	43.3; 47.7; 42.5	44.5	45.9	6.00; −3.77; 8.00
C10W60L2	72.1; 74.8; 78.4	75.1	66.0	−8.46; −11.76; −15.82
C10W65L1	44.9; 46.9; 45.2	45.7	42.2	−6.01; −10.02; −6.64
C10W65L2	65.3; 70.5; 71.6	69.1	60.2	−7.81; −14.61; −15.92
C10W70L1	40.6; 44.6; 41.6	42.3	39.0	−3.94; −12.56; −6.25
C10W70L2	63.1; 59.7; 55.7	59.5	57.1	−9.51; −4.36; 2.51
C15W50L1	42.6; 41.3; 41.3	41.7	45.2	6.10; 9.44; 9.44
C15W50L2	56.1; 49.4; 54.2	53.2	57.2	1.96; 15.79; 5.54
C15W55L1	40.4; 39.1; 40.0	39.8	42.2	4.46; 7.93; 5.50
C15W55L2	53.2; 51.6; 51.0	51.9	54.3	2.07; 5.23; 6.47
C15W60L1	37.5; 36.3; 36.8	36.9	39.2	4.53; 7.99; 6.52
C15W60L2	53.0; 49.0; 50.5	50.8	51.2	−3.40; 4.49; 1.39
C15W65L1	34.0; 33.0; 32.5	33.2	35.4	4.12; 7.27; 8.92

Table 7. *Cont.*

Specimen *	Experimental Compressive Strength (MPa)		Proposed Constitutive Model Compressive Strength (Mpa)	Error (%)
	Test	Avg. Value		
C15W65L2	47.9; 49.4; 49.4	48.9	47.5	−0.84; −3.85; −3.85
C15W70L1	32.9; 35.9; 36.1	35.0	33.4	1.52; −6.96; −7.48
C15W70L2	47.6; 47.7; 45.0	46.8	45.4	−4.62; −4.82; 0.89
				Average absolute error = 7.01

* C—circular concrete specimens; 15—diameter of circular (cm); W—w/c ratio (%); L—number of AFRP layers (1~3).

4.2. Constitutive Model for Axial STRAIN at the compressive Strength

As the axial stress of the cylindrical concrete reaches the compressive strength (f'_{cc}), the AFRP ruptures and cannot provide confinement stress. The axial strain of AFRP-confined concrete at the compressive strength is ε_{cc}', as shown in Figure 8. Therefore, the ε_{cc}' could be obtained from regression analysis and is expressed as Equation (7).

$$\varepsilon_{cc}' = \varepsilon_c' \left[1 + \alpha tan^2 \left(45^0 + \frac{\phi}{2} \right) \frac{f_l}{f_c'} \right] \tag{7}$$

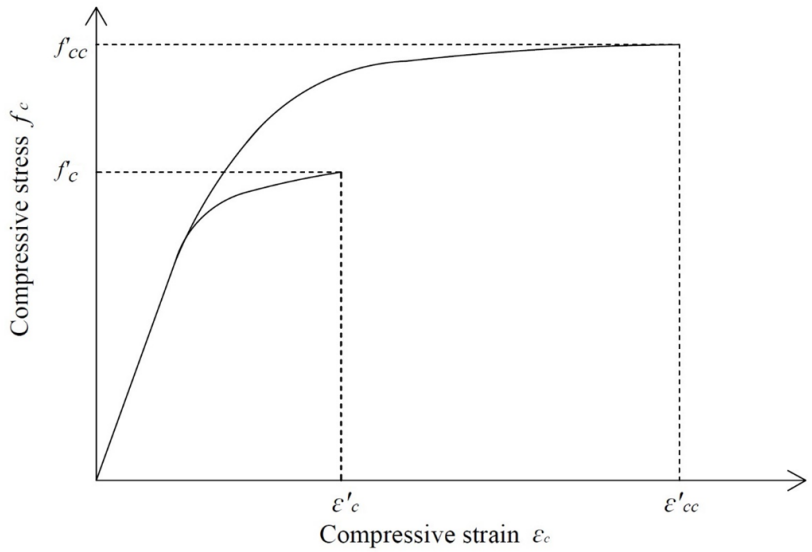

Figure 8. The stress–strain relationships of the cylindrical concrete specimens confined with and without AFRP.

As seen in Equation (7), the lateral confined stress (f_l) varies with the measured lateral strain (ε_{kf} on the AFRP, and it affects the axial strain ε_{cc}' of AFRP-confined concrete at the compressive strength). By substituting parameters ϕ, ε_c', ε_{cc}', f_l, and f_c' into Equation (7), the parameter α = 2.57 was determined from the regression analysis. The experimental strain of cylindrical concrete specimens was not uniform. Therefore, the coefficient of determination (R^2) for strain between the proposed constitutive model and the experimental result was 0.74.

The parabolic stress–strain relationship was adopted by some researchers [30,46], and it can be expressed as follows:

$$f_c = f_{cc}' \left[-\left(\frac{\varepsilon_c}{\varepsilon_{cc}'} \right)^2 + 2 \left(\frac{\varepsilon_c}{\varepsilon_{cc}'} \right) \right], \text{ where } 0 \leqq \varepsilon_c \leqq \varepsilon_{cc}' \tag{8}$$

Substituting the parameters f_{cc}' and ε_{cc}' of C10W70 from Table 7 into Equation (8), the stress–strain relationship of C10W70 confined with one, two, and three layers of AFRP confinement can be obtained, as shown in Figure 9.

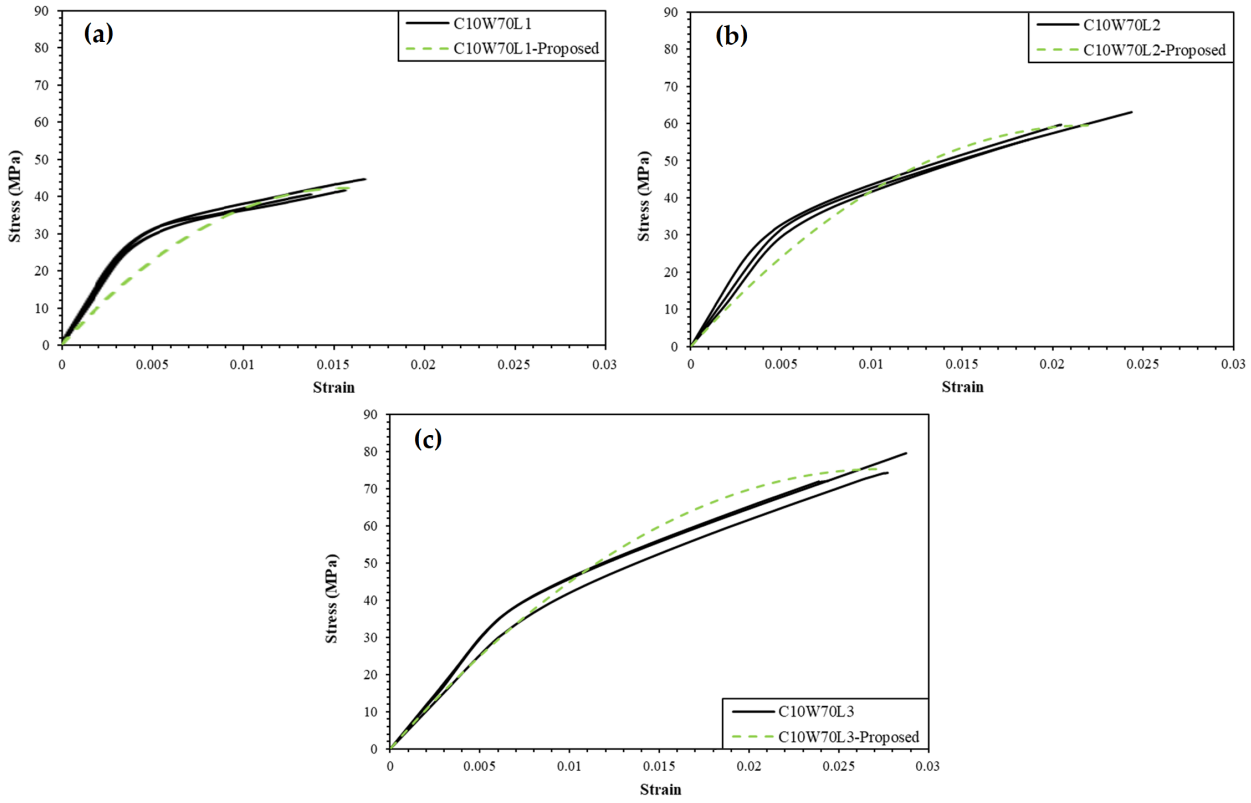

Figure 9. The experimental and proposed stress–strain relationships of C10W70 confined with 1, 2, and 3 layers of AFRP: (**a**) C10W70L1, (**b**) C10W70L2, and (**c**) C10W70L3.

4.3. Shape Factor for Square Cross-Section

As the experiment results shown in Table 6, the effectiveness of AFRP confinement for square cross-section concrete specimens was reduced compared with cylindrical concrete specimens. Therefore, it is necessary to design a new parameter, cross-section shape factor (k_c), for square cross-section concrete specimens. The shape factor (k_c) of the square specimens was defined as the ratio of effective confinement area (A_e) and section area (A), and it could be expressed as Equation (9), as shown in Figure 10.

$$k_c = \frac{A_e}{A} \geq 0 \tag{9}$$

The section area (A) is related to the length (d) and the radius of the chamfer (R_c) and can be expressed as Equation (10), and the effective confinement area (A_e) can be expressed as Equation (11), where d is the length of the square section, R_c is the radius of the chamfer, and θ is the intersect angle, as shown in Figure 10.

$$A = (d - 2R_c)^2 + 4(d - 2R_c) \times R_c + {R_c}^2 \times \pi \tag{10}$$

$$A_e = A - 4 \times \left(\left(\frac{\left(\frac{d-2R_c}{2}\right)}{cos(90^\circ - \theta)} \right)^2 \times \pi \times \frac{2\theta}{360} - \left(\frac{d - 2R_c}{2} \right)^2 \times tan(90^\circ - \theta) \right) \tag{11}$$

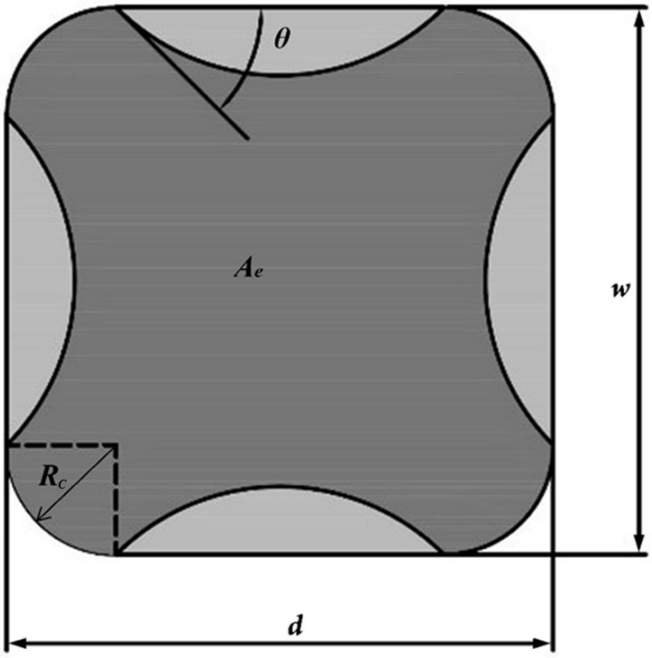

Figure 10. The effective confinement area of square cross-section concrete specimens.

4.4. Verification of the Constitutive Model

In this subsection, the material and dimension parameters of three-layer AFRP-confined cylindrical concrete specimens were substituted in Equation (3). The compressive strength of confined cylindrical concrete specimens predicted with the proposed constitutive model exhibit a good relationship with experimental results. Table 8 shows the predicted and experimental compressive strength of three-layer AFRP-confined cylindrical concrete specimens; the average absolute error was about 4.95%.

Table 8. Experimental and proposed constitutive model compressive strength of the specimens confined with three layers of AFRP confinement.

Specimen *	Experimental Compressive Strength (MPa)		Proposed Constitutive Model Compressive Strength (MPa)	Error (%)
	Test	Avg. Value		
C10W50L3	77.5; 80.9; 83.8	80.7	88.7	14.45; 9.64; 5.85
C10W55L3	88.5; 90.4; 86.2	88.4	85.6	3.28; −5.31; 0.70
C10W60L3	83.2; 90.6; 81.7	85.2	82.0	−1.44; −9.49; 0.37
C10W65L3	93.9; 84.9	89.4	78.3	−16.61; 7.77
C10W70L3	74.3; 79.6; 72.1	75.3	75.2	1.21; −5.53; 4.30
C15W50L3	65.1; 67.5; 65.4	66.0	69.3	6.45; 2.67; 5.96
C15W55L3	63.2; 65.4; 66.9	65.2	66.3	4.91; 1.38; −0.90
C15W60L3	63.2; 62.4; 60.3	62.0	63.3	0.16; 1.44; 4.98
C15W65L3	62.5; 58.0; 59.6	60.0	59.5	−4.80; 2.59; −0.17
C15W70L3	60.9; 62.6; 61.8	61.8	57.4	−5.75; −8.31; −7.12
				Average absolute error = 4.95

* C—circular concrete specimens; 15—diameter of circular (cm); W—w/c ratio (%); L—number of AFRP layers (1~3).

Figure 11 shows the coefficient of determination (R^2 = 0.906) between the proposed constitutive model predictions and the experimental results for AFRP-confined cylindrical concrete specimens. The results indicated that the proposed constitutive model can accurately predict the compressive strength of cylindrical concrete specimens confined with AFRP.

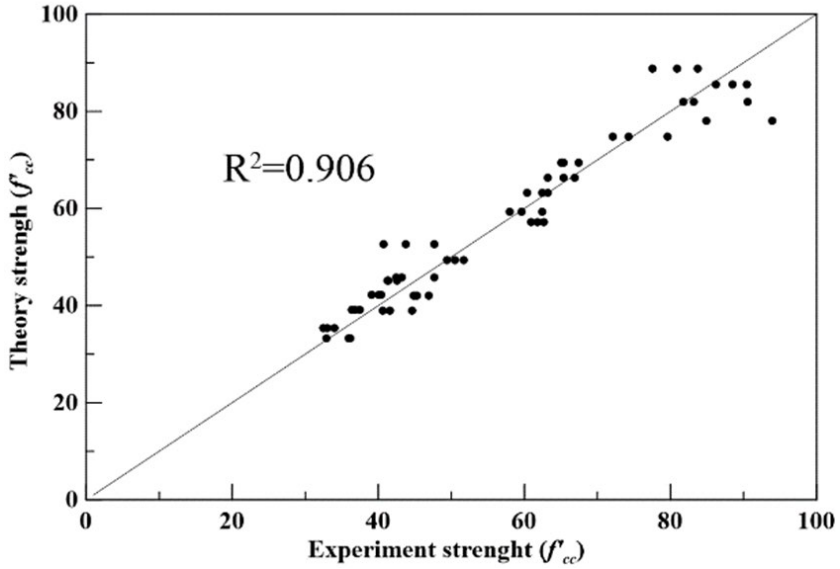

Figure 11. The coefficient of determination (R^2) of the proposed and experimental compressive strength of AFRP-confined cylindrical concrete specimens.

4.5. Predictions of Compressive Strength for Square Cross-Section Specimens

The studies reveal that the enhancing effect of compressive strength obtained by increasing the FRP confined rectangular or square cross-section concrete specimens was not as good as the effect of cylindrical specimens. According to previous studies [47–53], the enhancing effect of FRP-confined square specimens was decreased with decreasing ratio of the radius of the chamfer to the length.

The relationship between average absolute error and k_c is shown in Figure 12. The lowest absolute error was obtained when k_c = 0.52, which is substituted in Equation (9) to determine the corresponding intersect angle (θ).

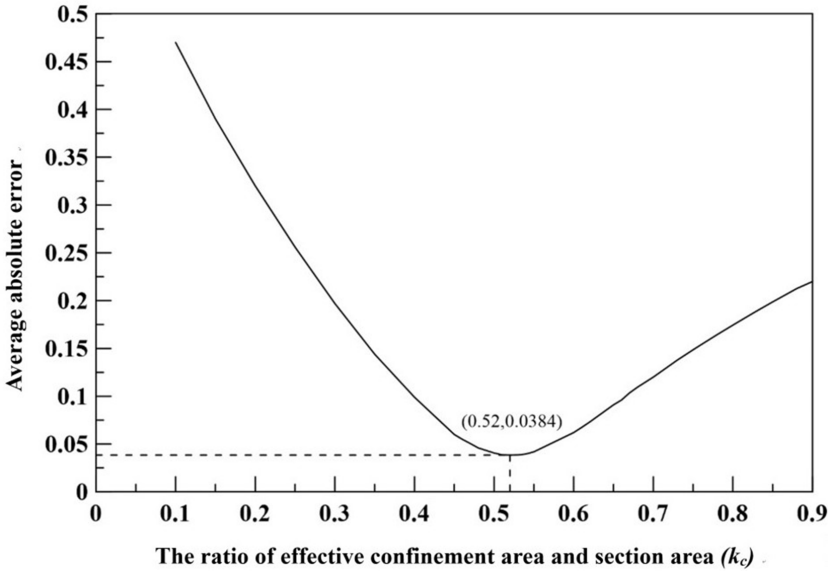

Figure 12. The relationship between average absolute error and different k_c.

Substituting the parameters d = 10 cm, R_c = 2 cm, and k_c = 0.52 into Equations (9) and (11), θ was obtained as 81°. The intersect angle of 81° was substituted into Equation (9), and then k_c could be expressed with Equation (12).

$$k_c = -1.1853 \times \left(\frac{2R_c}{d}\right)^2 + 2.4737\left(\frac{2R_c}{d}\right) - 0.281, \text{ where } \left(\frac{2R_c}{d}\right) \geq 0.121 \quad (12)$$

Substituting k_c into Equation (4), the effective lateral confined stresses for one to three layers of AFRP-confined square-section concrete specimens were 4.89 MPa, 9.78 MPa, and 14.67 MPa, respectively. Then, substituting the effective lateral confined stresses (f_l) into Equation (3), the compressive strength (f_{cc}') for square cross-section concrete specimens can be calculated using the proposed constitutive model as listed in Table 9. The average absolute error between experimental and predicted compressive strength was about 3.85%. Figure 13 shows the coefficient of determination (R^2 = 0.93) for the proposed constitutive model predictions and experimental compressive strength for AFRP-confined square cross-section concrete specimens. It can be concluded that the proposed constitutive model can accurately predict the experimental compressive strength.

Table 9. Experimental and proposed constitutive model compressive strength of the AFRP-confined square cross-section concrete specimens.

Specimen *	Experimental Compressive Strength (MPa)		Proposed Constitutive Model Compressive Strength (MPa)	Error (%)
	Test	Avg. Value		
S10W50L1	41.8; 41.6; 39.7	41.0	43.0	2.81; 3.31; 8.25
S10W50L2	50.8; 51.2; 52.5	51.5	52.9	4.04; 3.22; 0.67
S10W50L3	63.5; 64.1	63.8	62.7	−1.22; −2.15
S10W55L1	41.9; 38.8; 37.6	39.4	39.5	−5.77; 1.76; 5.01
S10W55L2	46.8; 48.9; 44.2	46.6	49.4	5.46; 0.93; 11.66
S10W55L3	61.9; 58.3; 62.2	60.8	59.2	−4.32; 1.59; −4.78
S10W65L1	34.9; 33.1; 34.1	34.0	34.2	−1.95; 3.38; 0.35
S10W65L2	44.2; 42.7; 44.9	43.9	44.1	−0.26; 3.38; −1.81
S10W65L3	59.3; 58.3; 57.2	58.3	54.0	−9.01; −7.45; −5.67
				Average absolute error = 3.85

* S—square cross-section concrete specimens; 10—edge length of square (cm); W—w/c ratio; L—number of AFRP layers (1~3).

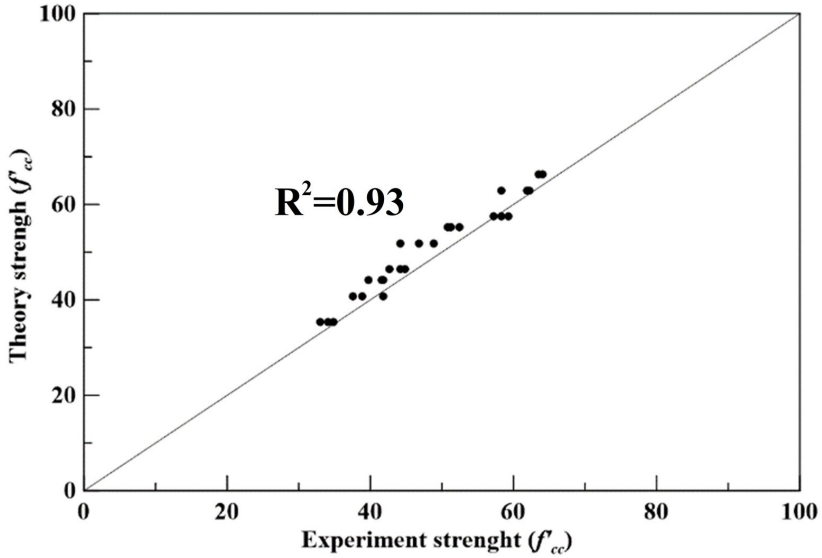

Figure 13. The coefficient of determination (R^2) for the proposed constitutive model and experimental compressive strength for square cross-section concrete specimens.

The accuracy of the proposed constitutive model was verified with five other researchers' experimental data, as shown in Table 10. The material parameters (E_f n, t, and ε_f), dimension (d and R_c), and strength (f_c') of the specimens were substituted into the proposed constitutive model. The average absolute errors were less than 6.38%. The proposed constitutive model can predict both the compressive strength of square concrete specimens confined with AFRP but also square-section concrete specimens confined with other types of FRP.

Table 10. The compressive strength of square concrete specimens from other researchers' experimental data and the proposed constitutive model.

Reference	FRP Type	Experimental Value			Proposed Constitutive Model				Error (%)
		d/h (Length/Height)	f'_c (MPa)	f'_{cc} (MPa)	R_c (mm)	Effective Area Ratio (%)	f'_l (MPa)	f'_{cc} (MPa)	
Wang and Wu, 2011 [14]	Aramid	100/300	46.4	49.5	10	11.95	1.99	50.5	2.02
			46.4	54.2			3.97	54.6	0.74
			46.4	59.0			5.96	58.6	−0.68
			78.5	78.7			1.99	82.6	4.96
			78.5	94.3			3.97	86.7	−8.06
			78.5	96.0			5.96	90.7	−5.52
			101.2	104.36			1.99	105.3	0.90
			101.2	112.06			3.97	109.4	−2.37
			101.2	110.87			5.96	113.4	2.28
									Average absolute error = 3.06
Wang and Wu, 2008 [49]	Carbon	150/300	31.9	33.6	15	16.6	1.27	34.5	2.68
			31.9	42.2	15	16.6	3.80	39.7	−5.92
			32.3	39.8	30	51.9	3.95	40.4	1.51
			32.3	56.5	30	51.9	11.84	56.5	0.00
			30.7	43.7	45	77.7	5.91	42.8	−2.06
			30.7	68.0	45	77.7	17.72	66.9	−1.62
			31.8	50.0	60	93.9	7.15	46.4	−7.20
			31.8	78.9	60	93.9	21.44	75.6	−4.18
			54.1	55.8	15	16.6	1.26	56.7	1.61
			54.1	59.4	15	16.6	3.79	61.9	4.21
			52.0	55.9	30	51.9	3.94	60.1	7.51
			52.0	63.0	30	51.9	11.81	76.2	20.95
			52.7	57.6	45	77.7	5.89	64.8	12.50
			52.7	80.3	45	77.7	17.68	88.9	10.71
			52.7	62.6	60	93.9	7.13	67.3	7.51
									Average absolute error = 6.01
Wu and Wei, 2010 [51]	Carbon	150/300	34.1	40.5	30	51.88	3.93	42.3	4.44
				40.7					3.93
				42.5					−0.47
									Average absolute error = 2.95
Al-Salloum, 2007 [47]	Carbon	150/500	34.8	48.3	25	41.2	7.32	49.8	3.11
			34.8	45.6	25	41.2	7.32	49.8	9.21
			29.0	57.0	38	66.8	11.88	53.3	−6.49
			29.0	55.0	38	66.8	11.88	53.3	−3.09
			27.5	61.7	50	84.1	14.96	58.1	−5.83
			27.5	63.7	50	84.1	14.96	58.1	−8.79
									Average absolute error = 6.09
Rousakis et al., 2007 [48]	G-glass	200/320	33.0	42.6	30	35.44	2.67	38.5	−9.62
			33.0	44.4			5.34	44.0	−0.90
			33.0	55.5			8.01	49.4	−10.99
			38.0	40.4			2.67	43.4	7.43
			38.0	52.8			5.34	48.9	−7.39
			38.0	60.2			8.01	54.4	−9.63
			39.9	43.1			2.67	45.4	5.34
			39.9	51.2			5.34	50.8	−0.78
			39.9	59.5			8.01	56.3	−5.38
									Average absolute error = 6.38

Table 11 lists the prediction models from recent researchers [14,17,18,41,42]. To verify the effectiveness of the proposed model, it is necessary to compare its performance with some models proposed by other researchers. The compressive strength of three layer KFRP confined cylindrical concrete specimens with dimensions of ϕ Ø 10 × 20 cm and Ø15 × 30 cm was tested and predicted.

Table 11. The prediction models from recent researchers.

Reference	Aspect Ratio (h/D)	Model
D. and K. [41]	Any ratio	$\frac{f'_{cc}}{f'_c} = 1 + 1.2\left(\frac{f_l}{f'_c}\right)^{1.25}\left(\frac{k_l}{f'_c}\right)^{0.37}$
L. and F. [18]	3.5 (750/200)	$\frac{f'_{cc}}{f'_c} = 1 + 3.1\left(\frac{f_l}{f'_c}\right)$
W. and W. [14]	Any ratio	$\frac{f'_{cc}}{f'_c} = \frac{\left(1.0+5.54\frac{f_l}{f'_c}\right)}{\sqrt{1+\frac{L-D}{353}\left(1-1.49\frac{f_l}{f'_c}\right)}}$
A. and G. [42]	Any ratio	$\frac{f'_{cc}}{f'_c} = 1 + \left(\frac{39}{ln^2(f'_c)}\right)^{1.25}\left(\frac{f_l}{f'_c}\right)$
V. and O. [17]	2 (305/152)	$f'_{cc} = f'_c\left(2.254\sqrt{1+\frac{7.94f_l}{f'_c}} - 2\left(\frac{f_l}{f'_c}\right) - 1.254\right)$

Table 12 shows the error analysis of compressive strength predictions for cylindrical concrete specimens confined with three layers of KFRP. The average absolute errors of other prediction models by [14,17,18,41,42] were 156.97%, 24.34%, 25.15%, 35.53%, and 45.52%, respectively. The compressive strengths between experimental results and the predictions made with the proposed constitutive model in this study were closer than others, and the average absolute error was 4.61%.

Table 12. The compressive strength error analysis of other prediction models.

Experiment		This Study		D. and K. [41]		L. and F. [18]		W. and W. [14]		A. and G. [42]		V. and O. [17]	
f'_c	f'_{cc}	f'_{cc} (MPa)	Error (%)	f'_{cc} (MPa)	Error (%)	f'_{cc} (MPa)	Error (%)	f'_{cc} (MPa)	Error (%)	f'_{cc} (MPa)	Error (%)	f'_{cc} (MPa)	Error (%)
34.44	80.75	88.69	9.83	58.50	−27.55	85.71	6.14	−34.79	−143.09	113.07	40.03	112.68	39.54
31.33	88.35	85.57	−3.15	56.84	−35.66	73.95	−16.29	−53.92	−161.03	115.48	30.70	105.57	19.49
28.71	85.16	82.04	−3.66	55.64	−34.66	69.23	−18.70	−72.79	−185.48	118.44	39.08	99.28	16.58
24.09	89.41	78.30	−12.43	54.12	−39.47	56.48	−36.84	−114.84	−228.44	126.70	41.71	87.40	−2.25
20.96	75.33	75.16	−0.23	53.70	−28.72	54.40	−27.78	−152.84	−302.90	135.71	80.16	78.63	4.38
33.11	65.95	69.28	5.05	45.89	−30.41	93.46	41.71	19.50	−70.44	87.02	31.95	95.71	45.12
30.15	65.16	66.31	1.76	43.70	−32.94	85.77	31.63	9.39	−85.59	87.84	34.81	90.07	38.23
27.12	61.97	63.27	2.10	41.59	−32.89	79.72	28.65	−2.65	−104.27	89.55	44.51	84.02	35.57
23.38	60.05	59.52	−0.88	39.24	−34.65	70.18	16.87	−20.85	−134.72	93.42	55.58	76.05	26.65
21.31	61.76	57.44	−6.99	38.11	−38.29	62.78	1.66	−33.17	−153.71	96.78	56.70	71.36	15.55
Avg. absolute error (%)			4.61		35.53		25.15		156.97		45.52		24.34

5. Conclusions

This study presents a constitutive model for the compressive strength of AFRP-confined concrete specimens of different cross-sections. The following conclusions were drawn based on the experimental results and the proposed constitutive model.

1. The experimental data of the specimens confined with one and two layers of AFRP were used to obtain the internal friction angle (ϕ). The average absolute error of compressive strength between the proposed constitutive model and experimental results was 7.01%, and the coefficient of determination (R^2) was 0.86;

2. The compressive strength of concrete specimens confined with three layers of AFRP were predicted using the above constitutive parameters; the absolute average error of cylindrical concrete specimens was less than 4.95%, and its coefficient of determination (R^2) was 0.906. Other researchers' experimental compressive strengths were predicted with the proposed constitutive model in this study, and the average absolute errors were less than 6.38%;
3. A cross-sectional shape coefficient for square cross-section concrete specimens was proposed and incorporated into the constitutive model, and the average absolute error for the predicted compressive strength and the experimental results was 3.83%; its coefficient of determination (R^2) was 0.93;
4. From the experimental results, AFRP confinement can enhance the compressive stress, corresponding compressive strain, and strain energy capacity of concrete specimens. This enhancement is attributed to the confinement effect facilitated via the AFRP;
5. The proposed constitutive model can predict the experimental maximum compressive strength for the normal strength concrete confined with AFRP composite materials with good accuracy. The major reason is that the compressive strength of the confined constitutive concrete was derived from the Mohr–Coulomb failure criterion with parameters obtained from the experimental data.

Author Contributions: Conceptualization, Y.-F.L.; Data curation, B.-Y.C. and J.-Y.S.; Formal analysis, B.-Y.C. and J.-Y.S.; Investigation, B.-Y.C. and G.K.R.; Methodology, Y.-F.L., C.-H.H. and M.-H.L.; Project administration, Y.-F.L. and C.-H.H.; Supervision, Y.-F.L. and W.-H.L.; Writing—original draft, B.-Y.C., J.-Y.S. and G.K.R.; Writing—review and editing, Y.-F.L., W.-H.L. and M.-H.L. All authors have read and agreed to the published version of the manuscript.

Funding: The authors are grateful for the support for this work provided by the Ministry of Science and Technology of the Taiwan government, under contract No. MOST-108-2218-E-027-005, and the "Research Center of Energy Conservation for New Generation of Residential, Commercial, and Industrial Sectors" from the Ministry of Education in Taiwan under contract No. L7121101-19.

Data Availability Statement: Data are contained within the article.

Conflicts of Interest: The authors declare no conflict of interest.

Nomenclature

A section area;
A_e effective confinement area;
C_0 uniaxial compressive strength without lateral confinement;
D diameter of the specimens;
d length of the square cross-section specimens;
E_{kf} elastic modulus of AFRP;
E_r average absolute error;
f'_c compressive strength of the unconfined concretes;
f'_{cc} compressive strength of the confined concretes;
f_c compressive stress of the concretes;
f_l effective lateral confined stress;
k_c cross-section shape coefficient;
m number of the compressive stress data recorded with the universal test machine;
n number of AFRP wrapping layers;
n_s number of the specimens;
R_c radius of the chamfer;
t thickness of a single AFRP layer;
V volume of the specimens;
x experimental compressive strength;
$\overline{x}$ average of experimental compressive strength;
y proposed compressive strength;
$\overline{y}$ average of proposed compressive strength.

ε_c	axial strain of AFRP-confined concrete;
ε_{cc}'	maximum axial strain of AFRP-confined concrete;
ε_i	compressive strain of the concrete specimens at point i;
ε_{kf}	ultimate lateral strain of KFRP;
θ	intersect angle;
σ_1	uniaxial compressive strength of rock;
σ_3	lateral confinement stress;
σ_i	compressive stress of the concrete specimens at point i;
ϕ	internal friction angle; and
Ø	diameter of the specimens.

References

1. Berthet, J.F.; Ferrier, E.; Hamelin, P. Compressive behavior of concrete externally confined by composite jackets. Part A: Experimental study. *Constr. Build. Mater.* **2005**, *19*, 223–232. [CrossRef]
2. Abbasnia, R.; Hosseinpour, F.; Rostamian, M.; Ziaadiny, H. Effect of corner radius on stress–strain behavior of FRP confined prisms under axial cyclic compression. *Eng. Struct.* **2012**, *40*, 529–535. [CrossRef]
3. Saleem, S.; Hussain, Q.; Pimanmas, A. Compressive behavior of PET FRP-confined circular, square, and rectangular concrete columns. *J. Compos. Constr.* **2017**, *21*, 04016097. [CrossRef]
4. Rousakis, T.C.; Panagiotakis, G.D.; Archontaki, E.E.; Kostopoulos, A.K. Prismatic RC columns externally confined with FRP sheets and pretensioned basalt fiber ropes under cyclic axial load. *Compos. Part B Eng.* **2019**, *163*, 96–106. [CrossRef]
5. Ceccato, C.; Teng, J.G.; Cusatis, G. Numerical prediction of the ultimate condition of circular concrete columns confined with a fiber reinforced polymer jacket. *Compos. Struct.* **2020**, *241*, 112103. [CrossRef]
6. Valasaki, M.K.; Papakonstantinou, C.G. Fiber reinforced polymer (FRP) confined circular concrete columns: An experimental overview. *Buildings* **2023**, *13*, 1248. [CrossRef]
7. Shawki Ali, N.K.; Mahfouz, S.Y.; Amer, N.H. Flexural Response of Concrete Beams Reinforced with Steel and Fiber Reinforced Polymers. *Buildings* **2023**, *13*, 374. [CrossRef]
8. Xian, G.; Guo, R.; Li, C. Combined effects of sustained bending loading, water immersion and fiber hybrid mode on the mechanical properties of carbon/glass fiber reinforced polymer composite. *Compos. Struct.* **2022**, *281*, 115060. [CrossRef]
9. Benzaid, R.; Mesbah, H.A. Chapter 6: Circular and Square Concrete Columns Externally Confined by CFRP Composite: Experimental Investigation and Effective Strength Models. In *Fiber Reinforced Polymers—The Technology Applied for Concrete Repair*; Masuelli, M.A., Ed.; IntechOpen: London, UK, 2013; Section 3; pp. 167–201. Available online: https://hal.science/hal-00782084v1/preview/InTech-Circular_and_square_concrete_columns_externally_confined_by_cfrp_composite_experimental_investigation_and_effective_strength_models.pdf (accessed on 10 October 2023).
10. Saeed, H.Z.; Khan, H.A.; Farooq, R. Experimental investigation of stress-strain behavior of CFRP confined Low Strength Concrete (LSC) cylinders. *Constr. Build. Mater.* **2016**, *104*, 208–215. [CrossRef]
11. Li, P.; Sui, L.; Xing, F.; Li, M.; Zhou, Y.; Wu, Y.F. Stress-strain relation of FRP-confined predamaged concrete prisms with square sections of different corner radii subjected to monotonic axial compression. *J. Compos. Constr.* **2019**, *23*, 04019001. [CrossRef]
12. Zhang, X.; Chen, P.; Wang, H.; Xu, C.; Wang, H.; Zhang, L. Constitutive model of FRP tube-confined alkali-activated slag lightweight aggregate concrete columns under axial compression. *Buildings* **2023**, *13*, 2284. [CrossRef]
13. Wu, H.L.; Wang, Y.F.; Yu, L.; Li, X.R. Experimental and computational studies on high-strength concrete circular columns confined by aramid fiber-reinforced polymer sheets. *J. Compos. Constr.* **2009**, *13*, 125–134. [CrossRef]
14. Wang, Y.F.; Wu, H.L. Size effect of concrete short columns confined with aramid FRP jackets. *J. Compos. Constr.* **2011**, *15*, 535–544. [CrossRef]
15. Ozbakkaloglu, T.; Lim, J.C.; Vincent, T. FRP-confined concrete in circular sections: Review and assessment of stress-strain models. *Eng. Struct.* **2013**, *49*, 1068–1088. [CrossRef]
16. Lim, J.C.; Ozbakkaloglu, T. Unified stress-strain model for FRP and actively confined normal-strength and high-strength concrete. *J. Compos. Constr.* **2015**, *19*, 04014072. [CrossRef]
17. Vincent, T.; Ozbakkaloglu, T. Compressive behavior of prestressed high-strength concrete-filled aramid FRP tube columns: Experimental observations. *J. Compos. Constr.* **2015**, *19*, 04015003. [CrossRef]
18. Lobo, P.S.; Faustino, P.; Jesus, M.; Marreiros, R. Design model of concrete for circular columns confined with AFRP. *Compos. Struct.* **2018**, *200*, 69–78. [CrossRef]
19. Sivasankar, S.; Sankar, L.P.; Kumar, A.P.; Shunmugasundaram, M. Compression behavior of cylinder reinforced with aramid fiber reinforced polymer. *Mater. Today Proc.* **2020**, *27*, 764–771. [CrossRef]
20. Product Manual. Zhe Jiang GBF Basalt Fiber Co., Ltd. Available online: http://www.chinagbf.com/product/584.html (accessed on 1 September 2023).
21. Li, Y.F.; Hung, J.Y.; Syu, J.Y.; Chang, S.M.; Kuo, W.S. Influence of sizing of basalt fiber on the mechanical behavior of basalt fiber reinforced concrete. *J. Mater. Res. Technol.* **2022**, *21*, 295–307. [CrossRef]
22. Chen, B.; Wu, K.; Yao, W. Conductivity of carbon fiber reinforced cement-based composites. *Cem. Concr. Compos.* **2004**, *26*, 291–297. [CrossRef]

23. Jung, S.H.; Kishimoto, H.; Nakazato, N.; Nakata, D.; Park, J.S.; Kohyama, A. Effect of the fabrication process on the microstructural evolution of carbon fibers and flexural property on C/SiC composites by the NITE method. *Ceram. Int.* **2022**, *48*, 32712–32722. [CrossRef]
24. Li, C.; Xian, G. Experimental and modeling study of the evolution of mechanical properties of PAN-based carbon fibers at elevated temperatures. *Materials* **2019**, *12*, 724. [CrossRef] [PubMed]
25. Pertuz-Comas, A.D.; Díaz, J.G.; Meneses-Duran, O.J.; Niño-Álvarez, N.Y.; León-Becerra, J. Flexural fatigue in a polymer matrix composite material reinforced with continuous Kevlar fibers fabricated by additive manufacturing. *Polymers* **2022**, *14*, 3586. [CrossRef] [PubMed]
26. Mander, J.B.; Priestley, M.J.N.; Park, R. Theoretical stress-strain model for confined concrete. *J. Struct. Eng.* **1988**, *114*, 1804–1826. [CrossRef]
27. Mander, J.B.; Priestley, M.J.N.; Park, R. Observed stress-strain behavior of confined concrete. *J. Struct. Eng.* **1988**, *114*, 1827–1849. [CrossRef]
28. Mirmiran, A.; Shahawy, M. Behavior of concrete columns confined by fiber composites. *J. Struct. Eng.* **1997**, *123*, 583–590. [CrossRef]
29. Razvi, S.; Saatcioglu, M. Confinement model for high-strength concrete. *J. Struct. Eng.* **1999**, *125*, 281–289. [CrossRef]
30. Li, Y.F.; Lin, C.T.; Sung, Y.Y. A constitutive model for concrete confined with carbon fiber reinforced plastics. *Mech. Mater.* **2003**, *35*, 603–619. [CrossRef]
31. Lin, C.T.; Li, Y.F. An effective peak stress formula for concrete confined with carbon fiber reinforced plastics. *Can. J. Civ. Eng.* **2003**, *30*, 882–889. [CrossRef]
32. Li, Y.F.; Fang, T.S. A constitutive model for concrete confined by steel reinforcement and carbon fiber reinforced plastic sheet. *Struct. Eng. Mech.* **2004**, *18*, 21–40. [CrossRef]
33. Li, Y.F.; Sio, W.K.; Tsai, Y.K. A compressive peak strength model for CFRP-confined thermal insulation materials under elevated temperature. *Materials* **2020**, *13*, 26. [CrossRef] [PubMed]
34. Li, Y.F.; Sio, W.K.; Yang, T.H.; Tsai, Y.K. A constitutive model of high-early-strength cement with perlite powder as a thermal-insulating material confined by carbon fiber reinforced plastics at elevated temperatures. *Polymers* **2020**, *12*, 2369. [CrossRef]
35. Wang, Z.; Wang, D.; Smith, S.T.; Lu, D. CFRP-confined square RC columns. I: Experimental investigation. *J. Compos. Constr.* **2012**, *16*, 150–160. [CrossRef]
36. Sadeghian, P.; Rahai, A.R.; Ehsani, M.R. Effect of fiber orientation on compressive behavior of CFRP-confined concrete columns. *J. Reinf. Plast. Compos.* **2010**, *29*, 1335–1346. [CrossRef]
37. Sadeghian, P.; Fam, A. Improved design-oriented confinement models for FRP-wrapped concrete cylinders based on statistical analyses. *Eng. Struct.* **2015**, *87*, 162–182. [CrossRef]
38. Keshtegar, B.; Sadeghian, P.; Gholampour, A.; Ozbakkaloglu, T. Nonlinear modeling of ultimate strength and strain of FRP-confined concrete using chaos control method. *Compos. Struct.* **2017**, *163*, 423–431. [CrossRef]
39. Khorramian, K.; Sadeghian, P. New mechanics-based confinement model and stress–strain relationship for analysis and design of concrete columns wrapped with FRP composites. *Structures* **2021**, *33*, 2659–2674. [CrossRef]
40. Toufigh, V.; Toufigh, V.; Saadatmanesh, H.; Ahmari, S.; Kabiri, E. Behavior of polymer concrete beam/pile confined with CFRP sleeves. *Mech. Adv. Mater. Struct.* **2019**, *26*, 333–340. [CrossRef]
41. Djafar-Henni, I.; Kassoul, A. Stress-strain model of confined concrete with Aramid FRP wraps. *Constr. Build. Mater.* **2018**, *186*, 1016–1030. [CrossRef]
42. Arabshahi, A.; Gharaei-Moghaddam, N.; Tavakkolizadeh, M. Development of applicable design models for concrete columns confined with aramid fiber reinforced polymer using Multi-Expression Programming. *Structures* **2020**, *23*, 225–244. [CrossRef]
43. De Luca, A.; Nanni, A. Single-parameter methodology for the prediction of the stress-strain behavior of FRP-confined RC square columns. *J. Compos. Constr.* **2011**, *15*, 384–392. [CrossRef]
44. Diboune, N.; Benzaid, R.; Berradia, M. New strength–strain model and stress–strain relationship for square and rectangular concrete columns confined with CFRP wraps. *Mech. Adv. Mater. Struct.* **2022**, *30*, 2971–2994. [CrossRef]
45. *ASTM C39/C39M-01*; Standard Test Method for Compressive Strength of Cylindrical Concrete Specimens. ASTM: West Conshohocken, PA, USA, 2021.
46. Kent, D.C.; Park, R. Flexural Members with Confined Concrete. *J. Struct. Div. ASCE* **1971**, *97*, 1969–1990. [CrossRef]
47. Al-Salloum, Y.A. Influence of edge sharpness on the strength of square concrete columns confined with FRP composite laminates. *Compos. Part B Eng.* **2007**, *38*, 640–650. [CrossRef]
48. Rousakis, T.C.; Karabinis, A.I.; Kiousis, P.D. FRP-confined concrete members: Axial compression experiments and plasticity modelling. *Eng. Struct.* **2007**, *29*, 1343–1353. [CrossRef]
49. Wang, L.M.; Wu, Y.F. Effect of corner radius on the performance of CFRP-confined square concrete columns: Test. *Eng. Struct.* **2008**, *30*, 493–505. [CrossRef]
50. Wu, H.L.; Wang, Y.F. Experimental study on reinforced high-strength concrete short columns confined with AFRP sheets. *Steel Compos. Struct.* **2010**, *10*, 501–516. [CrossRef]
51. Wu, Y.F.; Wei, Y.Y. Effect of cross-sectional aspect ratio on the strength of CFRP-confined rectangular concrete columns. *Eng. Struct.* **2010**, *32*, 32–45. [CrossRef]

52. Belouar, A.; Laraba, A.; Benzaid, R.; Chikh, N. Structural performance of square concrete columns wrapped with CFRP sheets. *Procedia Eng.* **2013**, *54*, 232–240. [CrossRef]
53. Nisticò, N.; Pallini, F.; Rousakis, T.; Wu, Y.F.; Karabinis, A. Peak strength and ultimate strain prediction for FRP confined square and circular concrete sections. *Compos. Part B Eng.* **2014**, *67*, 543–554. [CrossRef]